JGR Solid Earth

RESEARCH ARTICLE
10.1029/2021JB023722

Evaluating the Tsunamigenic Potential of Buried Versus Trench-Breaching Megathrust Slip

Matías Carvajal[1,2], Tianhaozhe Sun[3], Kelin Wang[3,4], Haipeng Luo[4,5], and Yijie Zhu[4]

[1]Instituto de Geografía, Pontificia Universidad Católica de Valparaíso, Valparaíso, Chile, [2]Programa de Doctorado en Ciencias Geológicas, Facultad de Ciencias Químicas, Universidad de Concepción, Concepción, Chile, [3]Pacific Geoscience Centre, Geological Survey of Canada, Sidney, BC, Canada, [4]School of Earth and Ocean Sciences, University of Victoria, Victoria, BC, Canada, [5]Now at Department of Earth and Planetary Sciences, McGill University, Montréal, QC, Canada

Key Points:

- Tsunamigenic seafloor uplift due to megathrust slip reflects a trade-off between rigid-body translation and elastic thickening
- Moderately buried slip is usually more tsunamigenic than trench-breaching slip of the same size, because of enhanced elastic thickening
- What determines tsunami size, such as in the 2011 Tohoku-oki tsunami, is mainly how large, not just how shallow, the offshore slip is

Supporting Information:

Supporting Information may be found in the online version of this article.

Correspondence to:

M. Carvajal and T. Sun,
matias.carvajal.ramirez@gmail.com;
tianhaozhe.sun@nrcan-rncan.gc.ca

Citation:

Carvajal, M., Sun, T., Wang, K., Luo, H., & Zhu, Y. (2022). Evaluating the tsunamigenic potential of buried versus trench-breaching megathrust slip. *Journal of Geophysical Research: Solid Earth*, *127*, e2021JB023722. https://doi.org/10.1029/2021JB023722

Received 29 NOV 2021
Accepted 14 AUG 2022

Abstract Subduction megathrust ruptures that breach the trench, such as in the 2011 $M = 9$ Tohoku-oki earthquake, can be very tsunamigenic. However, whether buried ruptures are intrinsically less tsunamigenic has not been fully investigated. Here, we conduct this investigation by studying the mechanics of seafloor deformation and the resultant tsunami runup. With a trench-breaching rupture, deformation is dominated by the rigid-body translation of the frontal upper plate, and seafloor uplift is enhanced by the horizontal motion of the sloping seafloor. With a buried rupture, the rigid-body motion is reduced, but the shortening of the upper plate due to seaward slip termination causes elastic thickening to enhance tsunamigenic seafloor uplift. By combining a finite-element deformation model and a shallow-water equation tsunami model, we systematically test various subduction zone geometrical and slip parameters to study the trade-off between rigid-body translation and elastic thickening in causing seafloor uplift and tsunami runup. To isolate the effect of slip depth, we compare scenarios with the same peak slip and rupture width. We find that very shallow ruptures, including those breaching the trench, are generally less tsunamigenic than deeper ruptures. Given peak slip, tsunamigenic potential is maximized if the rupture is not too shallow or too deep but is buried to moderate depths. Our model tests using variable hypothetical rupture depths suggest that, with a slip magnitude as large as in the 2011 Tohoku-oki earthquake, tsunami runups as high as the observed would occur even if the rupture were fully buried.

Plain Language Summary During subduction earthquakes, sudden seafloor deformation due to megathrust slip raises seawater to generate tsunamis. If the slip breaches the trench, seawater is raised by the seaward motion of the sloping seafloor. If the near-trench part of fault refuses to slip, in a scenario called buried rupture, the seafloor will bulge to raise seawater. Here we combine computer models of seafloor deformation and tsunami propagation to study how the two types of rupture control tsunami runup. We find that, given slip size and location, their tsunamigenic potential is similar owing to a trade-off mechanism. With buried rupture, tsunami generation is weakened by lessened motion of the sloping seafloor but strengthened by increased seafloor bulging. The effect is the opposite for a trench-breaching rupture. We also find that if a rupture is buried to an optimal moderate depth, the bulging effect and tsunami size are maximized. These findings clarify that the key reason for a large tsunami is how large, not just how shallow, the megathrust slip is. This knowledge helps to understand why some recent megathrust earthquakes, including the 2011 $M = 9$ Tohoku-oki earthquake, were so tsunamigenic. For tsunami hazard assessment, the tsunamigenic potential of buried ruptures should not be underrated.

1. Introduction

Earthquakes that rupture the very shallow part of subduction megathrusts can be very tsunamigenic, especially those that breach the trench (Cheung et al., 2022). The most notable examples include tsunami earthquakes that rupture the shallowest part of the megathrust (Hill et al., 2012; Kanamori, 1972; Satake, 1994) and the 2011 $M = 9$ Tohoku-oki earthquake in which large slip extended to the trench (Kodaira et al., 2021). It is understood that trench-breaching slip can displace large volumes of water to cause a large tsunami because of the seaward motion of the sloping seafloor (Hooper et al., 2013; Sun et al., 2017; Tanioka & Satake, 1996) and because of the large water depths around the trench (Geist et al., 2006; Polet & Kanamori, 2000). However, it is not well understood whether a buried rupture not extending to the trench, as reported for many other subduction earthquakes, is generally or always less tsunamigenic than a trench-breaching rupture with the same slip magnitude. Although

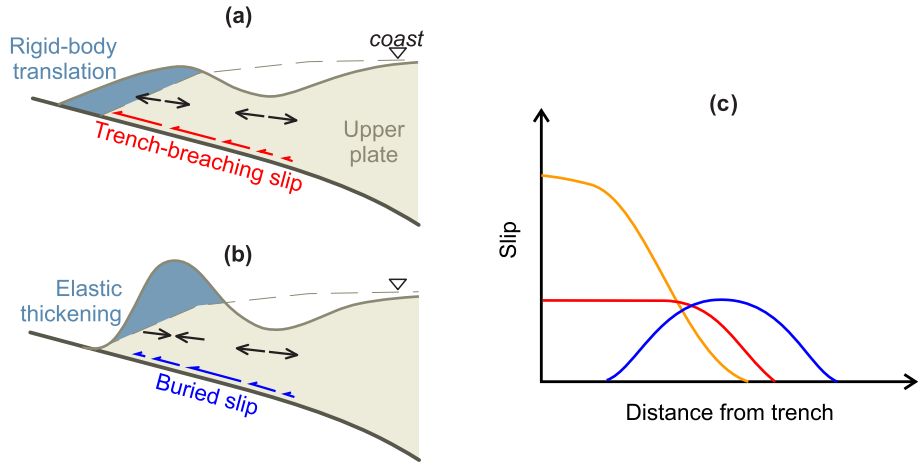

Figure 1. Cartoon illustrating the trade-off between the two mechanisms that control tsunamigenic seafloor deformation in trench-breaching and buried ruptures. (a) Dominance of rigid-body translation in trench-breaching rupture. The blue shaded area illustrates the enhanced near-trench seafloor uplift due mainly to the horizontal motion of the sloping seafloor. (b) Dominance of elastic thickening in buried rupture. The blue shaded area illustrates the enhanced seafloor uplift due mainly to the horizontal contraction and resultant thickening of the upper plate. Dashed line indicates pre-earthquake seafloor geometry. (c) Possible slip distributions for the two types of rupture. In this study, we compare models with identical peak slip, such as those shown in red and blue. The orange distribution may have the same moment as the blue distribution if the shallow rigidity is proportionally smaller, but the two are not compared because of their different peak slip values.

shortage of near-field, seafloor observations often causes large uncertainties in the reported presence or absence of near-trench slip, there is theoretical expectation that in some situations coseismic slip tapers toward the trench due to fault zone friction properties (Ikari et al., 2011; Scholz, 1998; Wang & Hu, 2006). Understanding the tsunamigenic potential of buried ruptures has both scientific and societal implications.

If large coseismic slip of the megathrust occurs at the trench, seafloor deformation is dominated by the rigid-body translation of the frontal wedge of the upper plate, and seafloor uplift is enhanced by the horizontal motion of the sloping seafloor (Figure 1a). However, if the slip is buried and tapers toward the trench (Figure 1b), seafloor uplift is not necessarily smaller. In this situation, the frontal part of the overlying upper plate is horizontally shortened, and consequent elastic thickening can lead to large seafloor uplift (Figure 1b). How these two deformation components, namely rigid-body translation and elastic thickening, contribute to tsunamigenic seafloor uplift in different rupture scenarios is the focus of this study. We employ finite element models of elastic deformation that include long-wavelength surface geometry appropriate for subduction zones. Using seafloor deformation predicted by these models as tsunami sources, we simulate tsunami wave propagation and runup at the model coast.

In comparing different rupture scenarios, we use the same maximum slip to isolate the effect of slip depth. In doing so, we are generally not comparing earthquakes with the same seismic moment which is a product of rock rigidity, slip, and rupture area. For example, if the rigidity of the frontal wedge material is very low (e.g., Geist & Bilek, 2001; Sallarès & Ranero, 2019; Satake, 1994), the slip distribution represented by the blue curve in Figure 1c may have a larger seismic moment than the red curve but the same moment as the orange curve. In this situation, our comparison is made between the blue and red curves because they have the same maximum slip. Besides, in assessing tsunami hazard on a local coastal area, if the anticipated rupture is long in the strike dimension such as in the 2004 $M = 9.2$ Sumatra, 1960 $M = 9.5$ Chile, and 1700 $M \approx 9.0$ Cascadia earthquakes, it is the fault slip directly offshore that is important (Williamson et al., 2019; Witter et al., 2013), not the moment of the earthquake which also includes slip elsewhere along strike.

By fixing the peak slip, we examine how seafloor geometry, fault geometry, and slip distribution affect the relative contribution of the two deformation components illustrated in Figures 1a and 1b to influence the main tsunami wave parameters that determine runup. We will show that the enhanced uplift due to the rigid-body translation of the sloping seafloor is at the price of much reduced elastic thickening, and vice versa, and we explore how this trade-off is modulated by geometrical and slip parameters. By shifting a slip model of the 2011

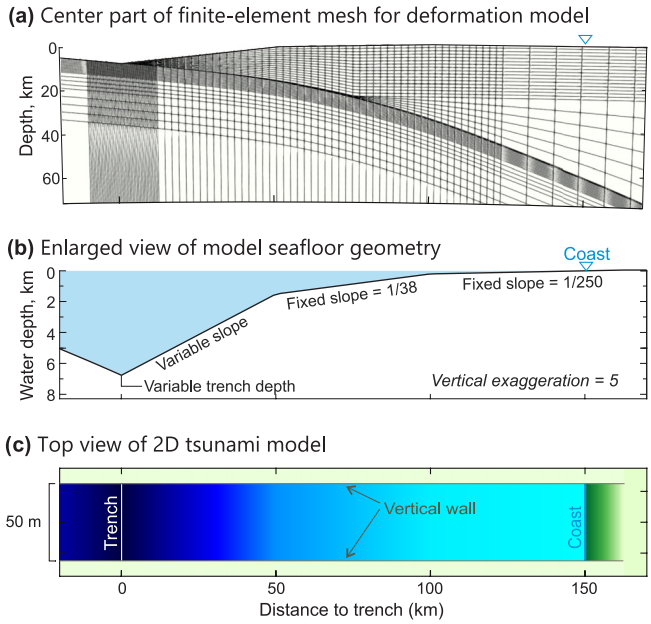

Figure 2. Illustration of the 2-D models used for surface deformation and tsunami modeling. (a) Center part of the finite-element mesh for subduction zone deformation models. The model is run in a spherical-Earth coordinate system, so that the depth axis and radial mesh lines are not strictly vertical in this display. (b) Vertically exaggerated seafloor geometry consisting of linear segments of different slopes. The shallowest segment extends landward of the coast to allow inundation and runup calculation. (c) 2-D channel used for tsunami modeling (width exaggerated 500 times). The model grid consists of 50×50 m^2 square cells, but only one row is needed in the strike direction.

Tohoku-oki earthquake to hypothetical greater depths along the Japan Trench megathrust, we will demonstrate that a rupture buried to a moderate depth can produce tsunami runups as large as those observed in 2011 along the coastal area facing the main rupture zone.

2. Methods of Deformation and Tsunami Modeling

2.1. Finite Element Modeling of Tsunamigenic Seafloor Deformation

2.1.1. The Subduction Zone Deformation Model

We employ a simple subduction zone geometry that reflects the main characteristics of many real subduction zones (Figure 2a). To focus on the main physical process, we ignore along-strike variations in most of our test models. In our modeling, the trench-coast distance is fixed at 150 km, and the trench depth varies in the range 3,300–10,300 m. The megathrust geometry shown in Figure 2a is typical of many subduction zones, but we will also vary the average dip of the fault in some models for testing purpose.

The model seafloor, from the coast to the trench axis, consists of three linear segments (Figure 2b). Each segment is 50 km long, and they together represent the general shape of real active continental margins. The shallowest segment, with its seaward limit at ~200 m below sea level and a slope of 1/250 (~0.2°), represents the continental shelf and extends landward of the coast to allow tsunami inundation on land (see Section 2.2). The middle segment, with a slope of 1/38 (~1.5°), extends 100 km offshore to a depth of ~1,500 m below sea level. The deepest and most seaward segment represents the lower continental slope and defines the upper surface of the frontal wedge. Because we are particularly interested in the impact of the sloping seafloor on tsunami generation (Figure 1a), we vary the slope angle of this segment over a range of 1/10 to 1/5.8 (2°–10°) in different models to cover the observed range at subduction margins. With the slope break fixed at 1,500 m below sea level, the variations in the lower slope lead to the variations in trench depth mentioned above. Seaward of the trench, we allow the seafloor to slope toward the trench as in real subduction zones (Figures 2a and 2b).

We use the finite-element code PGCviscl-3D, which has been extensively benchmarked against analytical solutions and used in our earlier subduction zone earthquake cycle models (Hu & Wang, 2012; Luo & Wang, 2021; Sun et al., 2014, 2018; Wang et al., 2012), to simulate the tsunamigenic seafloor deformation. The models considered in this work are purely elastic with prescribed fault slip (see Section 2.1.2). Potential permanent deformation of parts of the upper plate in the form of localized faulting or distributed plastic yielding adds further complications in real earthquakes (e.g., Hananto et al., 2020; Tsuji et al., 2013) but are ignored in our modeling because of the focus of this study. For simplicity, we assume a uniform model domain with Poisson's ratio 0.25, except for special tests. If megathrust slip distribution is kinematically prescribed, rigidity plays little role in controlling model deformation, as graphically illustrated in Figures S1 and S2 of Supporting Information S1. For a uniform model neglecting gravity, different rigidity values yield identical deformation results. Our models include the effect of gravity except for the illustrations in Figure S2 of Supporting Information S1, but the effect is negligibly small. Given slip distribution, the presence of low-rigidity materials in the frontal wedge or shallow crust (e.g., Sallarès & Ranero, 2019) only slightly affects predicted seafloor deformation (Figure S2 in Supporting Information S1).

We set the lateral boundaries more than 1,000 km away from the model rupture area and the bottom boundary at 600 km depth. The boundaries are adequately distant so that they do not affect model results in our region of interest. Our code models deformation in a spherical Earth, but a Cartesian system will yield nearly identical results for this spatial scale. There is no strictly 2-D model in a spherical Earth, but we still call our models with no along-strike variations 2-D models.

The deformation models yield three-component coseismic surface displacements. To obtain the added seafloor uplift due to the horizontal motion of the sloping seafloor (Figure 1a), we use the method of Sun et al. (2017) to derive the bathymetry difference before and after the rupture. For the smooth seafloor in our synthetic models (Sections 3 and 4), the approximate method of Tanioka and Satake (1996) will yield the same results. Because the main objective of this study is to investigate the trade-off between the two deformation components illustrated in Figure 1, it suffices to use a static model of instantaneous deformation. Potential contributions from realistic rise time and rupture propagation are of minor importance for this objective and are thus neglected.

2.1.2. Fault Slip Assignment

To focus on the main objective, we only consider megathrust ruptures that are completely offshore. In the suite of trench-breaching and buried rupture models that we use to investigate the aforementioned trade-off, the peak slip is 10 m, and the horizontal projection of the downdip rupture width is 100 km, both being representative of observed fault slip in M_w 8–8.5 megathrust earthquakes (Allen & Hayes, 2017). Although seafloor deformation scales linearly with slip magnitude, the resultant tsunami runups do not, because of the nonlinear nature of tsunami propagation and runup. Therefore, we do not normalize any of our model results using the peak slip value. Nonetheless, the knowledge learned from the 10 m slip models is qualitatively applicable to models of other slip values.

Figure 3a (green curves) shows the slip distribution in typical trench-breaching and buried rupture scenarios used in our models. Deformation and tsunami results for these models will be discussed in Section 3.1. The slip in the buried rupture follows a modified version of the bell-shape function of Freund and Barnett (1976) proposed by Wang and He (2008) with typographic errors fixed in Wang et al. (2013). This function depicts slip that tapers smoothly both updip and downdip. It also allows the bell-shaped slip distribution to be skewed updip or downdip, which will be dealt with in Section 4.4. Trench-breaching slip is modeled by replacing the updip limb of the bell-shape function with part of a sinusoidal function that allows the slip to decrease smoothly toward the trench (Gao et al., 2018). Different degrees of trench-breaching are represented by the amount of slip at the trench expressed as percentage of the peak slip at the apex of the bell-shape slip function. For 100% trench-breaching, the peak slip is sustained all the way to the trench (Figure 3a).

The kinematic slip distributions in Figure 3 are based on fault mechanics arguments and evolved from the classical 2-D crack model. The crack model assumes uniform stress drop in the rupture zone and zero slip elsewhere, resulting in abrupt termination of slip at the two edges of the rupture with stress singularities (e.g., Geist & Dmowska, 1999; Rudnicki & Wu, 1995). To suppress the unphysical singularities, Freund and Barnett (1976) kinematically modified the crack-model slip distribution to allow gradual termination of the slip at the two edges. Using an elastostatic finite element model including a frictional subduction fault, Wang and He (2008) simulated fault slip distribution and resultant tsunamigenic seafloor deformation by changing the fault friction coefficient to represent coseismic weakening or strengthening behavior. Because of their focus on the updip edge of the rupture, Wang and He (2008) allowed the singular behavior at the downdip edge of their rupture, similar to the classical crack model. They confirmed the validity of the bell-shape slip distribution of Freund and Barnett (1976) but found it to be more sharply peaked than in the friction model. They thus modified the Freund and Barnett (1976) slip by introducing another parameter to control the sharpness/flatness of the bell peak, resulting in the type of bell-shape distribution used by Ref2 (Figure 3a). If the classical crack model for a thrust fault breaks the "trench," fault slip gradually increases toward, and becomes nearly constant near the trench (Geist & Dmowska, 1999; Wang & He, 2008). This is the theoretical background for the 100% trench-breaching models in this and other (Carvajal, Cisternas, & Catalán, 2017; Gao et al., 2018) papers. Using a friction model similar to Wang and He (2008), Hu and Wang (2008) showed how the degree of trench breaching in megathrust slip is controlled by the degree of coseismic strengthening of the near-trench part of the fault. Their results provided theoretical basis for the models of variable degrees of trench breaching to be examined in Section 3. The buried slip and trench-breaching slip scenarios used in this paper can also be produced using dynamic rupture models that simulate rupture propagation and associated seismic waves (e.g., Kozdon & Dunham, 2013; Prada et al., 2021; Ramos & Huang, 2019). Given medium properties (e.g., rigidity distribution), regardless of how the rupture process is modeled, the final (net) fault slip uniquely determines the static seafloor deformation.

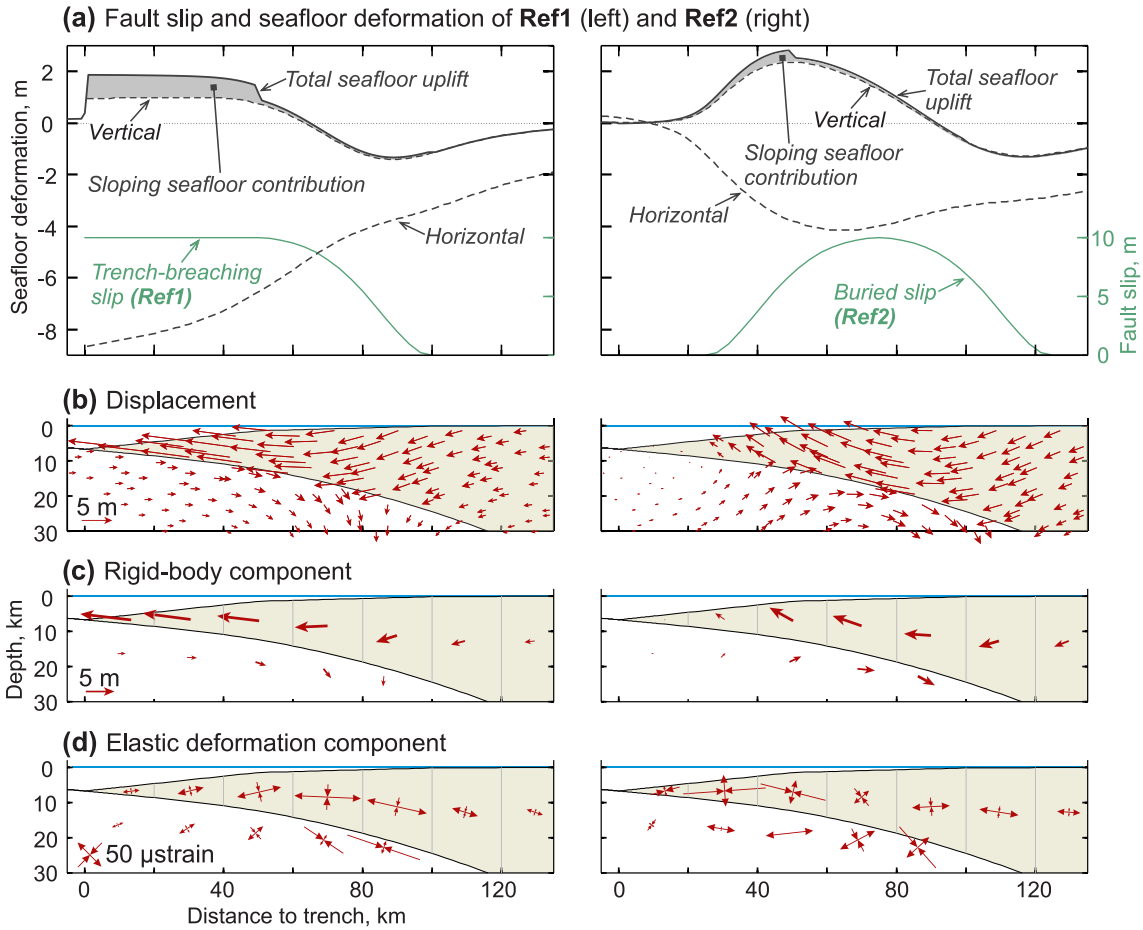

Figure 3. The two reference models Ref1 (left) and Ref2 (right). (a) Fault slip distribution (axis to the right) and seafloor deformation (axis to the left). "Sloping seafloor contribution" is the contribution to total seafloor uplift from the seaward translation of the sloping seafloor. (b) Displacement field. Displayed displacement vectors are randomly selected. The horizontal and vertical components along the top surface are shown in (a) using dashed lines. (c) Rigid-body component of the upper plate shown with translation vectors. (d) Elastic deformation component shown with principal strains. In (c and d), the deformation components are averaged over 20-km-wide blocks of the upper plate (block boundaries indicated by gray vertical lines) and shown at the center of each block.

2.2. Tsunami Modeling

The seafloor deformation predicted by the deformation model described above is the tsunami source for our runup modeling. However, the size of the runup is determined not only by the tsunami source but also by the tsunami propagation path from the source area to the coast (e.g., Geist, 1998). Specifically, for a given tsunami source, the propagation path modulates the shape of the incident leading wave as it propagates toward the coast and hence determines runup on land. All our source models except for a few in Section 5.2 produce a trough-leading wave because the megathrust rupture is sufficiently far offshore, such that the runup increases with the characteristic wavelength, trough amplitude, and frontal steepness of the leading wave (e.g., Geist, 1998; Satake et al., 2013; Tadepalli & Synolakis, 1994).

To isolate the effect of the tsunami source on runup, we try to minimize the effect of the propagation path in causing differences between different models. Therefore, we use identical seafloor geometry for distances >50 km from the trench in all our models (Figure 2b). However, we must vary the near-trench seafloor slope because it is an important parameter in our source study. The variation in frontal seafloor slope is accompanied with a variation in the water depth in the source region which also affects runup (Geist, 2002; Mulia et al., 2022), but its effect is expected to be small compared to the effect of the tsunami source. Based on our modeling experience, we are confident that the runup differences between different models predominantly reflect differences in the source, not in the propagation path. We have also run models in which the seafloor geometry at >50 km distance from the trench is slightly different from that shown in Figure 2b, such as with a steeper or flatter slope for the middle

segment or around the coast, but still identical between different models. The results (not displayed) verify that what we learn about the source effect from the models in Sections 3 and 4 is not fundamentally changed.

We use the widely adopted Kajiura transfer function (Kajiura, 1963) to convert the static seafloor deformation to sea surface deformation which provides the initial condition for tsunami propagation. The 2-D Kajiura function approximates the attenuation of short-wavelength components through the water column, leading to a smoother sea surface elevation. The effect is particularly obvious in trench-breaching rupture scenarios in which the displacement discontinuity at the trench richly produces short-wavelength components (Felix et al., 2021). For simplicity, we use a constant water depth—the trench depth—in the function, despite the presence of seafloor slope. We have verified that using different reference water depths makes only slight differences to the tsunami model results and does not affect our conclusions.

We use modeling software COMCOT (Cornell Multi-grid Coupled Tsunami model; Wang & Power, 2011) to compute sea-surface elevations during tsunami propagation and inundation from the source area to the farthest point inland where runup is calculated. COMCOT adopts explicit staggered leap-frog finite difference schemes to solve the two-dimensional Linear and Nonlinear nondispersive Shallow Water Equations in either spherical (Section 5.2) or Cartesian (Sections 3, 4 and 5.1) coordinates. Because a few of our tsunami source models produce relatively short tsunami waves compared to the local water depth and thus push the theoretical performance limits of COMCOT which does not include the effect of frequency dispersion, we conducted tests using a more sophisticated code NEOWAVE (Yamazaki et al., 2011). NEOWAVE includes a vertical velocity term to handle dispersive tsunami waves and a shock capturing scheme to handle very steep wave front in runup calculation, both at the cost of computing time. With a comprehensive comparison of the performance of COMCOT against NEOWAVE (see Text S1 in Supporting Information S1), we found that for our source models and the relatively short trench-coast distance, the two codes yield very similar results (Figure S3 in Supporting Information S1). We therefore decided to use COMCOT for efficiency and convenience.

A subduction zone deformation model without along-strike variations is called a 2-D model. However, because of the absence of depth dimension in the mathematical formulation of depth-averaged shallow-water equation models, a tsunami wave model based on such a 2-D deformation source is commonly referred to as a one-dimensional (1-D or 1-DH) tsunami model. Nonetheless, in this paper we refer to this type of tsunami model also as 2-D, to be compatible with its 2-D deformation source. Similarly, a tsunami model based on a 3-D deformation source such as for any real earthquake is therefore called a 3-D tsunami model in this paper, despite the fact that it is strictly a 2-D or 2-DH model.

Our 3-D tsunami modeling follows a standard procedure (e.g., Carvajal and Gubler, 2016; Carvajal, Cisternas, & Catalán, 2017; Wang & Power, 2011). Our 2-D tsunami models, in which the tsunami propagates only in the strike-normal direction, use a special design to enhance computing efficiency, so that we can readily run hundreds of models using a laptop computer to investigate the physical process. Only a distilled set of models are shown in this paper. For these 2-D models, we use a 228-km-long channel discretized into squared grid cells of 50×50 m^2, with 4,559 grid cells in the strike-normal direction and only 1 in the strike direction (Figure 2c). We apply an absorbing boundary condition to the open ocean end of the model and use the moving boundary scheme (implemented in COMCOT) at the landward wet-dry boundary to track the moving shoreline and simulate inundation and runup. We use the Nonlinear Shallow Water Equations and incorporate the effects of bottom friction along the channel using a Manning's roughness coefficient of 0.025 s m$^{-1/3}$ (Kotani et al., 1998). The computation time step is set to satisfy the Courant-Friedrichs-Lewy stability condition of the finite difference method and varies from 0.07 to 0.14 s. All simulations are run for 1 hr tsunami propagation time, which is more than adequate to capture the maximum model runup (associated with the leading wave).

3. Tsunami Generation by Trench-Breaching and Buried Ruptures

3.1. Trade-Off Between Rigid-Body Translation and Elastic Thickening

Here we use the two reference models shown in Figure 3, namely Ref1 and Ref2, to explain the trade-off between the two deformation components illustrated in Figure 1. The effects of various geometrical and slip parameters on this trade-off will be systematically studied in Section 4. Figure 3a shows their slip distribution (green) and resultant surface deformation (black), and Figure 3b shows the displacement field in cross-section view. In Figure 3a, the vertical and horizontal components of the seafloor displacement (Figure 3b) are illustrated using dashed lines.

The total tsunamigenic seafloor uplift, which includes the contribution from the horizontal motion of the sloping seafloor (shaded area), is illustrated using a solid line.

In understanding the results in Figure 3, we need to consider the horizontal and vertical components of the rigid-body translation separately. The presence of the vertical component is because of the dip of the fault. The vertical (upward) translation contributes to both Ref1 and Ref2, but the difference in tsunamigenic seafloor deformation between these two models primarily reflects the trade-off between the horizontal rigid-body translation and elastic thickening. In Ref1, the horizontal motion of the sloping seafloor contributes to about 50% of the total uplift but there is no contribution from elastic thickening. On the other hand, in Ref2, thickening due to elastic shortening causes large seafloor uplift, but the sloping-seafloor contribution is greatly diminished.

To better explain this trade-off, we separately illustrate the rigid-body translation component (Figure 3c) and the elastic deformation component (Figure 3d) averaged over 20-km-wide blocks of the upper plate, with the translation vector and the principal strains shown at the center of each block. The translation vector is simply the average of a dense grid of displacement vectors within each block. The strain tensor is derived by fitting a model of constant strain to all these displacement vectors; averaging strain tensors of individual finite elements in the block will yield nearly identical results. The domination of one of the two deformation components in each model is clear. Rigid-body translation near the trench approaches the value of fault slip in Ref1 but is zero in Ref2 (Figure 3c). This causes the large near-trench seafloor uplift in Ref1 but not in Ref2 (Figure 3a). In Ref1, the trenchward decrease in the stiffness of the wedge-shaped frontal upper plate causes the horizontal displacement to increase trenchward despite the uniform fault slip in this area (Figure 3a). The consequent horizontal extension causes slight thinning of the upper plate (Figure 3d), so that the contribution of elastic thickening to seafloor uplift is actually negative. In Ref2, the updip tapering of the fault slip (Figure 3a) leads to horizontal shortening, and the resultant thickening (Figure 3d) gives rise to large seafloor uplift peaking at the location where the slip gradient is the highest (Figure 3a).

3.2. The Mechanism of Elastic Thickening

The horizontal motion of the sloping seafloor in the trench-breaching model is straightforward to understand, but the mechanism of elastic thickening in the buried rupture model requires further explanation. To illustrate the mechanism, we show the deformation due to bell-shape slip along a hypothetical horizontal fault in an elastic half space (Figure 4). The use of a horizontal fault eliminates any uplift due to the upward rigid-body translation of the hanging wall. The model-predicted surface uplift (and subsidence) is therefore purely a consequence of elastic deformation. Drawing an analogy to our 2-D megathrust models (Figure 3), we call the portion of the slip zone to the left of the peak slip the "updip" segment of the rupture, and the portion to the right the "downdip" segment. In Figure 4, all distances are normalized using W_u, the width of the updip segment. For simplicity, we assume a symmetric slip distribution (Figure 4a), such that the deformation is antisymmetric with respect to the location of the peak slip, but a skewed slip distribution would demonstrate the same mechanical principles.

The model displacement field around the center of the rupture zone exhibits opposite horizontal motion of the hanging wall and footwall (Figures 4d–4f). While their relative motion is determined by the assigned slip magnitude, the absolute motion of each side (i.e., relative to its pre-rupture position) is governed by their stiffness contrast. For a shallowly buried fault, the thin hanging wall is much less stiff than the footwall, resulting in much greater leftward motion of the former than the rightward motion of the latter (Figures 4d–4f). Consequently, the part of the hanging wall overlying the updip segment of a shallowly buried rupture suffers greater shortening than for a more deeply buried rupture. If the rupture were extremely deeply buried, such as to a depth 10 times the rupture width, the opposite displacements of the hanging wall and footwall would be similar in size.

In these models, the amount of surface uplift caused by the horizontal shortening of the hanging wall depends on the slip gradient, the depth of the fault, and the Poisson's ratio.

The effect of the slip gradient does not require explanation and illustration. It is self-evident that a sharper tapering of the slip causes greater shortening and hence more uplift. An extreme example commonly seen in the literature is the uplift spike caused by a sudden updip termination of fault slip (infinite slip gradient), an artifact in numerous tsunami source models, especially those that use uniform-slip rectangular fault segments with their updip edges buried at small depths.

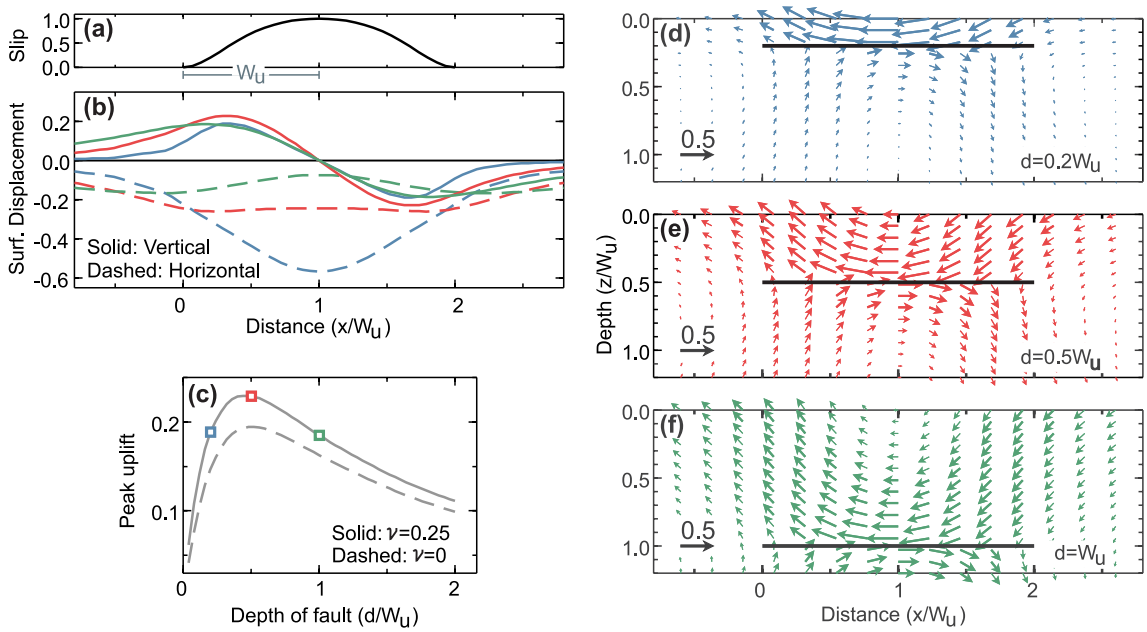

Figure 4. Model deformation due to buried rupture on a hypothetical horizontal fault to illustrate the mechanism of elastic thickening. (a) Slip distribution normalized by peak slip. Hanging wall moves to the left. W_u is the width of the "updip" segment of the slip zone. (b) Surface displacements of the three color-coded models shown in (d–f). (c) Peak surface uplift (normalized by peak slip) as a function of fault depth d (normalized by W_u) for two Poisson's ratio values (ν), showing that the highest peak uplift occurs when fault depth $d = 0.5W_u$. Results for the three models in (d–f) are shown with color-coded squares. (d–f) Cross section view of displacement vectors for three models with different fault depths.

The effect of fault depth is more complex. As discussed above, given slip distribution, there is greater shortening if the fault is shallower. However, surface uplift is an integrated effect of vertical strain over a depth range. If the fault is too shallow, despite the large shortening, the integrated effect of thickening over the small depth range it too small to cause large uplift (Figure 4d). Conversely, if the fault is too deep, although the effect of thickening is integrated over a greater depth range, the horizontal shortening is too small to cause much thickening (Figure 4f). Therefore, there is an optimal depth that maximizes surface uplift. Our systematic model tests show the optimal depth to be $0.5W_u$ (Figure 4c). The scaling between W_u and the optimal fault depth for elastic thickening is fundamental to tsunamigenic seafloor uplift. Although it cannot be directly applied to a curved dipping fault, the physics behind this scaling dictates that a rupture buried at moderate depths has a greater tsunamigenic potential than very deeply or very shallowly buried ruptures. In a theoretical study of tsunami energy, Ward (1980) found an optimal depth of 5 km for a hypothetical point source. Our optimal depth for a finite fault is only for elastic thickening, and the maximization of tsunami energy will require additional factors. Nonetheless, in addition to maximizing the amplitude of the uplift, our optimal depth also appears to result in surface deformation with a steeper land-facing slope (Figure 4b) which, as discussed in Section 2.2, enhances tsunami runup.

The effect of the Poisson's ratio is minor. If we assume zero Poisson's ratio, the predicted uplift will only be slightly reduced (Figure 4c). Likewise (not displayed), if we assume a Poisson's ratio 0.5 (incompressible), the uplift will only be slightly enhanced. However, the demonstrated small role of the Poisson's ratio helps to clarify the mechanics that governs the uplift. It shows that the elastic thickening here is not a simple matter of compressing an elastic object in one direction causing it to expand in the orthogonal direction. Instead, it is the result of complex deformation. In simple words, as the hanging wall moves updip and encounters resistance due to the decrease and termination of fault slip, materials elastically "pile up" mostly by shear deformation to cause the surface to bulge. As reflected by the displacement vectors near the fault in Figures 4d–4f, the originally horizontal fault also endures some geometrical distortion in this process.

3.3. Tsunami Runup Due to Trench-Breaching and Buried Ruptures With the Same Peak Slip

Having explained the mechanics of seafloor uplift due to trench-breaching and buried ruptures, here we use the same examples Ref1 and Ref2 to calculate tsunami runup. The results shown in Figure 5 serve two purposes. First,

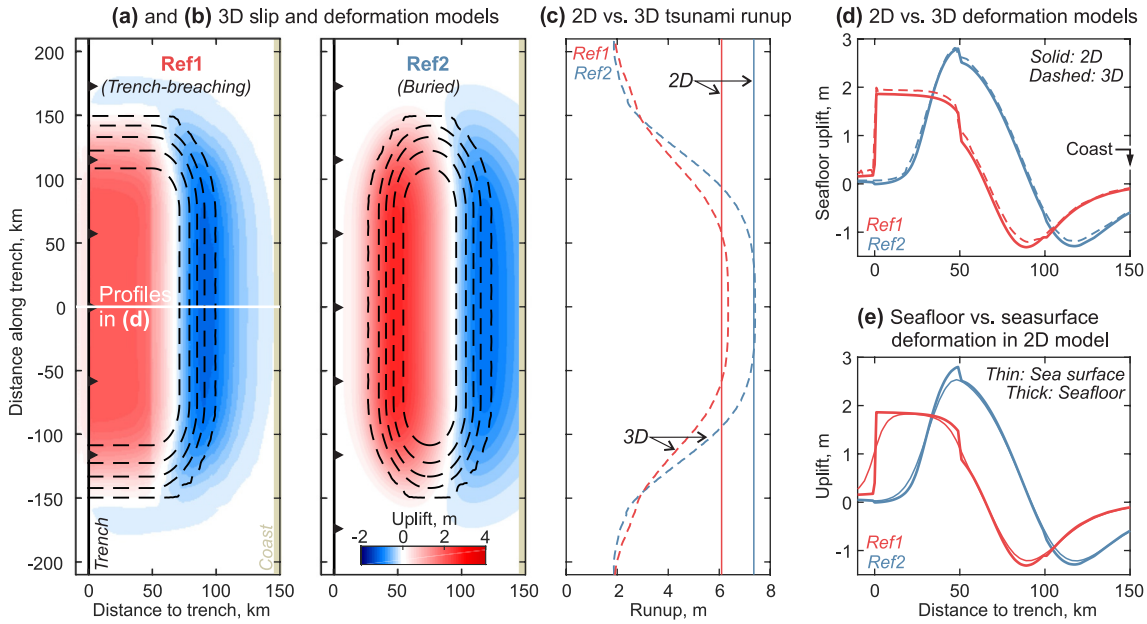

Figure 5. Tsunami source and corresponding runup for the two reference models and their 3-D variations. (a) Fault slip distribution (dashed contours at 2 m interval from 0 to 8 m) for a 3-D variation of Ref1 and its consequent seafloor deformation. The 3-D model is modified from Ref1 by limiting rupture length along strike as shown. (b) Similar to (a) but for Ref2. (c) Comparison of tsunami runup between the two reference models and between each model and its 3-D variation. (d) Comparison of seafloor uplift between the two reference models and between each model and uplift along the line of symmetry of its 3-D variation. (e) Comparison between seafloor and sea-surface deformation for both reference models. The smoother sea-surface deformation here and in (a and b) is obtained by applying the Kajiura (1963) transfer function to the seafloor deformation (see Section 2.2).

by comparison with 3-D results, they demonstrate the effectiveness of 2-D tsunami runup models in representing the primary physical process. Such a demonstration is important, because the exploration of the physical process in Section 4 will be carried out using 2-D models. Second, they demonstrate that a rupture buried to a moderate depth generates greater tsunami runup than does a trench-breaching rupture with the same peak slip. Besides, this is a convenient occasion to show how the Kajiura transfer function (Section 2.2) modifies seafloor uplift to yield sea surface uplift (Figure 5d).

In the two 3-D examples in Figure 5, fault slip in the dip direction is identical to the 2-D Ref1 and Ref2 models, but the along-strike rupture length is 300 km with slip smoothly terminating at the side edges. Figures 5a and 5b show their slip distribution and the resultant seafloor uplift in map view. Figure 5d shows that the seafloor uplift along the line of symmetry of the 3-D model (dashed) is very similar to what is predicted by the corresponding 2-D model (solid). Similarly, Figure 5c shows that the 3-D model tsunami runup within 50 km of the line of symmetry (dashed) is very similar to what is predicted by the corresponding 2-D model (solid). By systematically comparing 2-D runup models with 3-D models of different along-strike lengths (results not displayed), we find that the 2-D runup results rather accurately approximate 3-D results derived along the line of symmetry if the rupture lengths in the 3-D models are longer than the trench-coast distance.

Of greater importance to the theme of the present study is the impact of the trade-off between the two deformation components discussed above on tsunami runups. Contrary to what one may intuitively expect without doing the modeling, the buried rupture Ref2 causes a larger runup than the trench-breaching rupture Ref1. In terms of producing tsunamigenic seafloor uplift, the effect of the horizontal translation of the sloping seafloor in Ref1 fails to compete against the effect of the elastic thickening in Ref2. The peak slip in Ref2 occurs near the optimal depth $0.5W_u$ to maximize elastic thickening. Note that seafloor uplift in Ref2 occurs below shallower water depths than in Ref1, but it still produces a larger runup. This demonstrates that the runup differences between the two models are determined primarily by the different tsunami sources as controlled by the trade-off between the two deformation components, not by the different water depths and propagation paths (see Section 2.2).

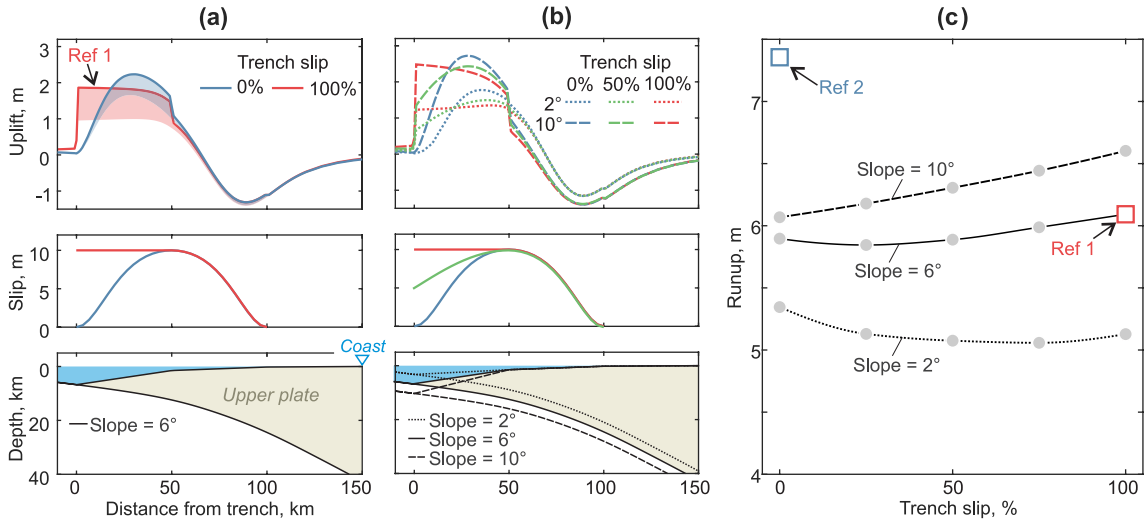

Figure 6. Test models to illustrate how tsunami runup due to trench-breaching rupture is affected by near-trench seafloor slope. (a) From bottom to top: model geometry, slip distribution, and seafloor uplift, coded by line color and style. Shaded areas in top panel show contributions to uplift from the horizontal motion of the sloping seafloor. (b) Similar to (a) but for a lower (2°) and higher (10°) near-trench seafloor slope. (c) Runup as a function of trench slip for the three different slopes shown in (a and b). Each circle represents a model test. The runup values produced by the two reference models are shown for comparison.

4. Factors That Influence the Relative Importance of Elastic Thickening and Rigid-Body Translation

In Section 3.3 (Figure 5), we showed that the trench-breaching model Ref1 is less tsunamigenic than the buried-rupture model Ref2. In this section we further investigate the competition of the two deformation components in a broader parameter space. The model tests summarized in Figures 6 and 7 show how geometrical factors may enhance or hinder tsunami runup caused by a trench-breaching rupture. Tests summarized in Figure 8 shows how the downdip distribution of slip (e.g., slip gradient) affects tsunami runup caused by a buried rupture. We again fix the peak slip at 10 m. We use the same width of the horizontal projection of the rupture for all the slip

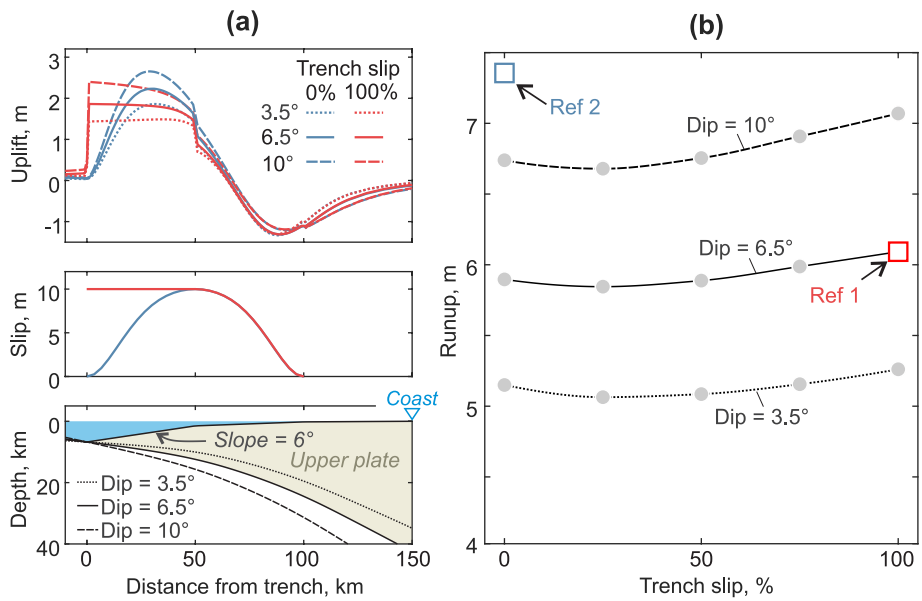

Figure 7. Test models to illustrate how tsunami runup due to trench-breaching rupture is affected by fault dip. (a) Similar to Figure 6b but for different values of fault dip averaged over the 0–50 km distance and for only the two end-member degrees of trench breaching (i.e., 0% and 100%). The value 6.5° has been used for all the models in Figures 3, 5 and 6. (b) Similar to Figure 6c but for the three fault dips shown in (a). The dip = 6.5° curve is identical to the slope = 6° curve in Figure 6c.

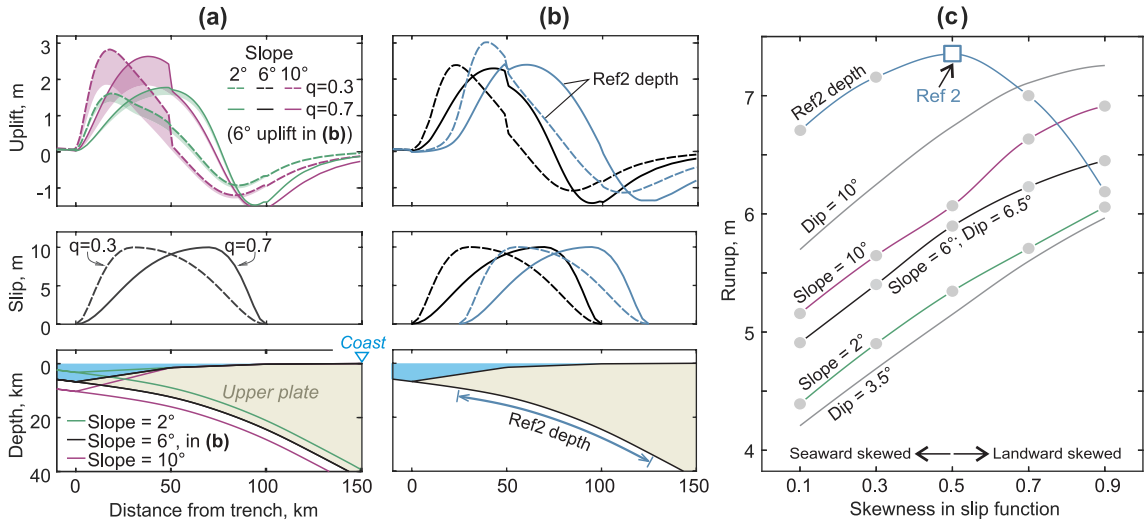

Figure 8. Test models to illustrate how tsunami runup due to buried rupture is affected by the skewness q of fault slip distribution. (a) Test models for different seafloor slope angles as in Figure 6. From bottom to top: model geometry, two slip distributions with $q = 0.3$ (dashed) and 0.7 (solid), and the resultant seafloor uplift with the shaded area indicating contribution from the horizontal motion of the sloping seafloor. (b) Models with the same seafloor slope (6°) but different rupture depths. One set of models (black) has the same shallow rupture depth as in (a), and the other set (blue) has the same rupture depth as Ref2 as shown in the bottom panel. (c) Runup as a function of slip skewness for the three seafloor slope angles in (a) and for the "Ref2 depth" models. Each circle represents a model test. The two gray lines with no circles show results for the 3.5° and 10° fault dips (see Figure 7). For each curve in this plot, if the seafloor slope or fault slip is not indicated, it means that the value is the same as for the black curve.

models in these tests to simplify parameter analyses, such that the buried ruptures shown in Figures 6–8 differ from Ref2 for being shallower. Therefore, unlike Ref2 (Figure 3a), the buried-rupture models in Figures 6–8 feature significant seaward translation of the sloping seafloor, although not as much as in trench-breaching models because of the diminishing fault slip toward the trench (Figure 6a). The models in Figures 6–8 illustrate how this effect is further strengthened or weakened at the cost or to the benefit, respectively, of elastic thickening.

4.1. Unimportance of Increasing the Degree of Trench Breaching Given Peak Slip

For demonstrating the trade-off between the two deformation components, the most illuminating is the stunningly small effect of increasing the degree of trench breaching in affecting tsunami runup shown by the many models summarized in Figures 6 and 7. Because the rigid-body translation of the sloping seafloor causes large near-trench uplift below deep water (Figure 1a), one might expect that a greater degree of trench breaching such as 100% (red curves in Figures 6a, 6b and 7a) would produce much larger runup. But quantitative modeling shows the effect to be very small. The results in Figures 6c and 7b show that the runup due to 100% trench slip is only slightly larger than 0% trench slip or in some situations even less.

The mechanical reason for the unimportance of increasing the degree of trench breaching in these models is explained in Section 3: an increase in the effect of rigid-body translation is always at the cost of elastic thickening. In Figure 6a, given seafloor slope, a larger trench slip leads to greater rigid-body translation and hence greater uplift near the trench, but at the same time the smaller elastic thickening leads to reduced uplift farther landward. Consequently, tsunami runup stays at a similar level regardless of the degree of trench breaching (the slope = 6° curve in Figure 6c). The fact that most of the curves in Figures 6c and 7b have a concave upward shape indicates that there usually is some "optimal" amount of trench slip that produces runup smaller than either 0% or 100% trench slip.

4.2. Effects of Near-Trench Seafloor Slope

Although the trade-off between the two deformation components tends to be balanced regardless of the degree of trench breaching, geometrical factors can slightly tip the balance. Steepening or flattening the near-trench seafloor slope will amplify or reduce, respectively, the contribution of the horizontal seafloor motion (Figure 6). This effect is most pronounced in trench-breaching ruptures with 100% trench slip which produce the largest

horizontal motion of the sloping seafloor. As discussed above, even for 0% trench slip, there is still significant horizontal motion of the sloping seafloor, although diminishing trenchward. Its contribution to seafloor uplift is larger if the seafloor slope is higher, as exemplified by runup values for the three models with 0% trench slip in Figure 6c. In this model setting, a greater seafloor slope also means a greater thickness of the upper plate, but the increase in the effect of elastic thickening on seafloor uplift is much less than that of the rigid-body translation. For example, for 100% trench slip, the effect of elastic thickening is negative (i.e., thinning) as shown in Figure 3c, which implies that in the high-slope examples in Figures 6b and 6c, the rigid-body translation effect overcompensates for the diminished elastic thickening effect to generate greater runup than in the lower-slope examples.

In the models shown in Figures 6b and 6a, a higher slope angle is accompanied with a greater water depth at the trench. Given the dominance of the trade-off effect between the two deformation components in this process (Figure 1), we do not deem it necessary to display results that separately illustrate the effect of seafloor slope and trench water depth in affecting tsunami runup due to trench-breaching slip.

4.3. Effects of Fault Dip

In Figure 7, we show models that are modified from those in Figure 6a by uniformly tilting the subducting plate around a pivot point at the trench which is fixed at a constant water depth. The models are named after the average fault dip over the 0–50 km distance (see bottom panel of Figure 7a). With other parameters fixed, an increase $\Delta\beta$ in fault dip β has two effects that both lead to greater tsunami runup, and both are explained by the deformation mechanisms described in Section 3 and Figures 3 and 4. First, it increases the thickness of the upper plate and hence the effect of elastic thickening (see Section 3.2 and Figure 4). Second, with a negligibly small decrease in the horizontal rigid-body translation, roughly by a factor of $(1 - \Delta\beta{\cdot}\beta) \approx 1$, it increases the upward rigid-body translation roughly by a factor of $(1 + \Delta\beta/\beta)$ and hence leads to greater seafloor uplift. Our model results indicate that, due to the combination of these two effects, a greater fault dip results in similar increase in seafloor uplift in all rupture models (Figure 7a) and hence an upward shift of the runup versus trench slip curve (Figure 7b).

4.4. Effects of Slip Distribution in Buried Ruptures

The results presented in Figures 6 and 7 show that, given peak slip, the degree of trench breaching has little impact on the tsunamigenic potential of megathrust ruptures. In particular, none of these models produces tsunami runup as high as in Ref2. Here we investigate what slip distribution makes a fully buried rupture more tsunamigenic. For this, we vary the skewness parameter q of the bell-shape slip distribution function (Wang et al., 2013) from 0.1 to 0.9 without altering the width of the rupture. This results in ruptures with shallower to deeper concentration of slip (Figure 8). We run the same tests for all the three near-trench seafloor slope angles in Figure 6 (Figure 8a). We also compare these models with those with the Ref2 rupture depth (Figure 8b).

The models in Figures 8a and 8b with the shallow (i.e., not Ref2) rupture depth demonstrate the importance of the shape of seafloor deformation in tsunami generation discussed in Section 2.2. In these models, slip skewness very weakly affects the contribution to uplift from the sloping seafloor (e.g., shaded areas in Figure 8a) but strongly affects how elastic thickening is accomplished. Recall that elastic thickening (or thinning) is controlled by the gradient and depth of the slip (Section 3.2). For these shallow ruptures, slip skewness affects not only the peak slip depth but also the slip gradient. In seaward skewed models (e.g., $q = 0.3$), elastic thickening due to the sharp updip slip gradient at a shallow depth causes large but narrow uplift near the trench, but elastic thinning due to the smoother downdip gradient at a greater depth causes small but broad subsidence closer to the coast. This combination results in seafloor deformation with a gentle land-facing slope between the peak uplift and peak subsidence. The landward skewed models (e.g., $q = 0.7$) are just the opposite. Their seafloor deformation features a broader seafloor bulge and a steeper land-facing slope—deformation characteristics that are well known to increase tsunami runup (Figure 8c) (Geist, 1998; Satake et al., 2013; Tadepalli & Synolakis, 1994). We have done the same tests for the three fault dips in Figure 7 (with the same seafloor slope angle 6°), and the results show the same effect of slip skewness on tsunami runup (Figure 8c). Therefore, for this model set up, no matter what geologically reasonable seafloor slope and fault dip we assume, a landward skewed rupture always produces greater tsunami runup. For the 10 m peak slip assumed in these models, the runup difference between the two end member skewness values $q = 0.1$ and 0.9 is around 1.5 m for any of our geometrical combinations (Figure 8c).

In comparison, the influence of the degree of trench breaching is much smaller. For example, even with a very high seafloor slope of 10°, increasing the trench slip from 0% to 100% of the peak slip of 10 m increases runup by only 0.5 m (Figure 6c).

Comparison with models of the Ref2 rupture depth (Figure 8b) demonstrates the role of rupture depth in controlling elastic thickening. In general, given slip skewness, a deeper rupture leads to a higher seafloor bulge and greater tsunami runup (Figure 8c). Exceptions occur if the slip is extremely landward skewed such as $q = 0.9$. In this situation, contribution from the limited horizontal motion of the sloping seafloor is still appreciable in the shallow-rupture model but almost absent in the model of Ref2 rupture depth. As a result, for $q = 0.9$, the "Ref2 depth" model produces even lower tsunami runup than the shallow-rupture model with the same seafloor slope (6°) and fault dip (6.5°) (black curve in Figure 8c)—a subtle display of the trade-off between the two deformation components discussed in Section 3. The "Ref2 depth" models in Figure 8b also illustrate the competing roles played by the size and shape of the seafloor deformation in tsunami generation. Here the symmetric slip (Ref2) leads to the highest runup (Figure 8c). Compared to Ref2, the seaward skewed models produce larger peak seafloor uplift, but the gentler land-facing slope of the seafloor bulge reduces its tsunamigenic potential. On the other hand, the landward skewed models produce a steeper land-facing slope of the seafloor bulge, but the smaller peak uplift reduces its tsunamigenic potential. For the landward skewed models, the propagation path effect discussed in Section 2.2 further reduces the tsunamigenic potential: the leading wave grows less as it propagates toward the coast because deformation occurs mostly under very shallow water or on land (Carvajal, Cisternas, Gubler, et al., 2017; Geist et al., 2006).

5. Discussion

5.1. Real-World Complexities

To focus on the main objective of this work, our modeling studies assume that the upper and lower plates are homogeneously elastic in the deformation process, that slip occurs only along the megathrust, and that the trench is not filled by large amounts of sediment. Other complications in the real world certainly also affect tsunami runup. For example, near-trench seafloor uplift can be enhanced by inelastic deformation of wedge sediments (Ma & Nie, 2019; Tanioka & Seno, 2001) or by slip diverted to steeper faults off the megathrust such as splay faults or frontal thrusts (Felix et al., 2021; Gao et al., 2018; Wang & Tréhu, 2016).

Despite these real-world complexities, much of the main message we have learned regarding the effect of slip depth on tsunamigenic seafloor deformation is still valid. For example, let us consider a subduction zone with a 2- or 5-km-thick sediment layer burying the trench (Figure 9a). The 5-km case is similar to what has been reported in southern Sumatra (Gulick et al., 2011). In these scenarios, if a trench-breaching rupture does happen, slip will have to be diverted from the megathrust to one or multiple frontal thrusts. For simplicity, let us follow Gao et al. (2018) to assume that all the slip is diverted to a hypothetical single frontal thrust along the full strike length of the megathrust rupture so that it can be represented by a 2-D model (lower panel in Figure 9a). Slip along the steeply dipping frontal thrust results in a spike in near-trench uplift, of which the amplitude and width increase with trench slip and sediment thickness, respectively (Figure 9a). The higher and the wider this near-trench uplift spike is, the larger its contribution to runup. As a consequence, with 100% of the peak slip diverted to the frontal thrust, the model with a 5-km sediment layer produces higher tsunami runups than those with 0 or 2 km sediment and even exceeds that of the buried-rupture model Ref2 (Figure 9b). However, if less than 50% of the peak slip is diverted to the frontal thrust, the resultant runup is still less than in Ref2.

The potency of Ref2 in producing large runup owes to the broad bulge farther landward due to enhanced elastic thickening (Figures 1b, 3a and 5c). As can be deduced from the frontal thrust rupture examples (Figure 9), other rupture scenarios involving near-trench complexities (e.g., Ma & Nie, 2019) would mostly affect shorter-wavelength deformation near the trench (Felix et al., 2021) and therefore be unable to produce the large tsunamigenic bulge as in Ref2. Therefore, it still holds that moderately buried ruptures such as Ref2 would usually be among the most effective in causing tsunami runups for a given slip magnitude.

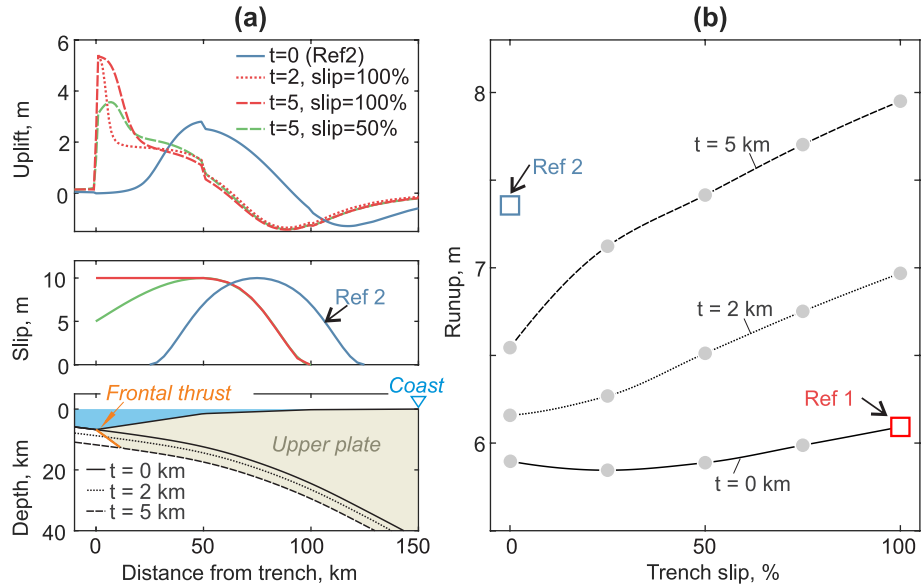

Figure 9. Test models to illustrate how trench-breaching rupture may occur to affect tsunami runup in the presence of thick sediment, in comparison with Ref2. (a) From bottom to top: model geometry, slip distribution, and seafloor uplift, coded by line color and style. In these models, the trench is assumed to be filled by a sediment layer of thickness t. Trench-breaching slip reaches the surface through a frontal thrust shown in orange in the lower panel. (b) Runup as a function of trench slip for the three different t values in (b). Each circle represents a model test. The $t = 0$ curve is identical to the slope = 6° curve in Figure 6c and the dip = 6.5° curve in Figure 7b.

5.2. Hypothetical Buried Large Ruptures in Japan Trench

The 2011 $M = 9$ Tohoku-oki earthquake ruptured to the trench with large slip and caused one of the largest tsunamis in history. There is little doubt that the very large slip magnitude in this earthquake is a key factor in causing the large tsunami (Kodaira et al., 2021), but the role of the very shallow depth and trench-breaching nature of the slip requires further quantitative testing. In this section, we design hypothetical slip distributions with the same peak slip but different degrees of trench breaching or different depths along the Japan Trench megathrust and compare their tsunami runup predictions. The set of hypothetical slip scenarios may pertain to past or future megathrust earthquakes in the Japan Trench subduction zone.

It is well known that the largest runups in the 2011 Tohoku-oki earthquake occurred north of 39°N, not in the region of main rupture (Figure S4 in Supporting Information S1) (Mori et al., 2011). The source for the largest runup in the north is still not fully understood (Kodaira et al., 2021), although some efforts have been made to explain it (e.g., Du et al., 2021; Satake et al., 2013; Yamazaki et al., 2018). We neither are in a position to tackle this scientific mystery. To focus on the main theme of this paper, we pay attention only to the coastal area directly facing the main rupture zone between 37.3 and 39°N where large trench-breaching slip occurred (Figure 10e and Figure S4 in Supporting Information S1).

We take the average slip distribution of 44 slip models for the 2011 Tohoku-oki earthquake in the literature (Wang et al., 2018) as the "original" model ("Trench-breaching (original)" in Figure 10), and modify it to produce two hypothetical sets of slip models. In one set, we modify the slip distribution seaward of the peak slip to let the slip breach the trench to different degrees, including 0% ("No trench-breaching" in Figure 10). In the other set, we systematically shift the original distribution downdip to greater depths to produce buried-rupture models with the same peak slip (e.g., "Moderately buried" in Figure 10). When doing the downdip shifting, we filled the originally non-existent part of the slip distribution seaward of the trench with slip values that smoothly taper to zero at or before reaching the trench (Figure S5 in Supporting Information S1). The slip distributions of all the eight test models are shown in Figure S5 of Supporting Information S1 in map and cross-section views.

For the 3-D tsunami modeling, we use a computational domain for the Japan Trench margin that encompasses the 2011 rupture area, extending from 36.5 to 40°N and 140.5 to 144.7°E (Figure S4a in Supporting Information S1). Because the experiment focuses on assessing the effect of the depth or trench-breaching nature of the slip on the

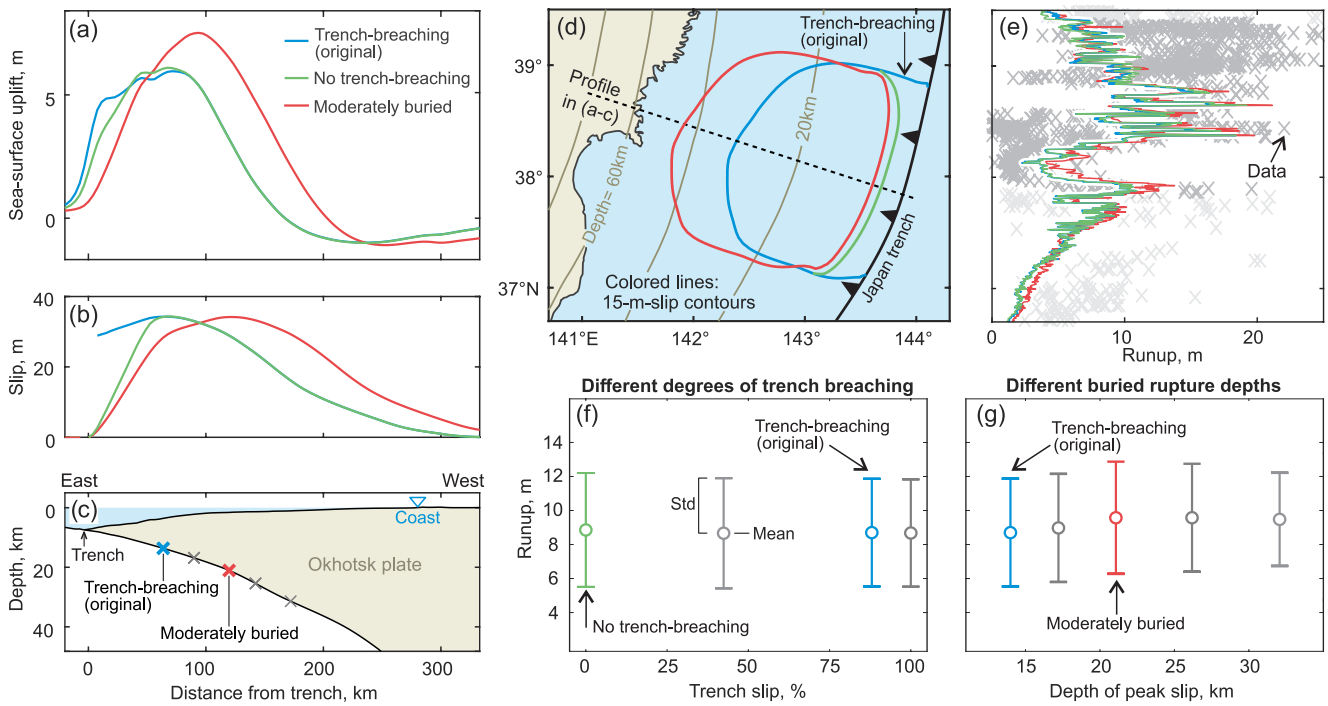

Figure 10. Numerical experiments to test the role of rupture depth in tsunami generation using Japan Trench topography, bathymetry, and fault geometry, and hypothetical variations of a slip model of the 2011 Tohoku-oki earthquake. (a) Sea surface deformation along the profile shown in (d) predicted by 3 of the 8 slip models tested in these experiments. (b) Fault slip distributions for the three models in (a) along the same profile, coded by line color and style. The original "Trench-breaching" slip model is the average of 44 Tohoku-oki slip models in the literature (Wang et al., 2018). "No trench-breaching" is modified from the original model by forcing the slip to taper to zero at trench. "Moderately buried" is constructed by shifting the original model downdip while allowing the slip to taper to zero at trench. (c) Fault geometry along the same profile and tested hypothetical depths of identical peak slip (crosses). (d) Map view of the three slip models in (b), represented by their (color coded) 15-m contours. (e) Tsunami runup predicted by the three (color coded) slip models in (d). The observed values (data) are from The 2011 Tohoku Earthquake Tsunami Joint Survey (TTJS) Group (2011) (http://www.coastal.jp/tsunami2011). (f) Runup predictions by models modified from the original model by forcing trench slip to be a fraction of the peak slip. (g) Runup predictions by models with the same value but different depths of peak slip. See (c) for peak slip depths.

overall tsunami size at the adjacent coast rather than assessing details of coastal hydrodynamics, it suffices to use the coarse bathymetry data from the GEBCO (2019) digital atlas which has a grid resolution of 15 arc-sec or ~500 m. We calculated tsunami propagation and runup using COMCOT with model parameters similar to those of the 2-D models described at the end of Section 2.2. Simulation time was 2 hr, adequate for modeling runup along the adjacent coast associated with the leading wave. Despite the simplicity of the model setup and the low-resolution of the elevation data in the coastal region, our model predicted runup using the averaged slip model of the 2011 Tohoku-oki earthquake (Wang et al., 2018) compare reasonably well with both the values of and along-shore variations in the observed runups of this event along the coast facing the main rupture zone (Figure 10c; Figure S4b in Supporting Information S1).

The results in Figure 10f show that, for fixed peak slip, whether fault slip breaches the trench and by what degree have little impact on tsunami runup. If anything, the "No trench-breaching" model, which is similar to a severely seaward skewed rupture model in Figure 8, produces a slightly higher average runup than any of the trench-breaching models.

The results in Figure 10g indicate that, given the same peak slip, trench-breaching shallow slip does not lead to the largest average runup. Instead, the buried rupture scenarios produce slightly higher tsunami runups owing to the effect of elastic thickening. These results further confirm what has been learned from our 2-D synthetic models discussed in Sections 3 and 4.

The results in Figure 10 collectively show that, in comparison with the slip magnitude, whether or not the slip is very shallow or trench-breaching is not a major factor affecting tsunami runup. The very large fault slip in the 2011 Tohoku-oki earthquake would have generated a very large tsunami even if the slip were not very shallow or trench-breaching. Because of the above explained purpose of this modeling experiment, we have used the same

peak slip for models of different rupture depths and do not address the question whether shallower ruptures tend to exhibit larger or smaller slip. What geological conditions might or might not give rise to these hypothetical scenarios is a different matter that is not discussed here.

5.3. Implications for Understanding Tsunami Earthquakes

Tsunami earthquakes produce larger tsunami runups than expected from their seismologically determined earthquake size (Kanamori, 1972). Based on independent seismic and geodetic evidence, it is clear that tsunami earthquakes indeed feature very shallow, and possibly trench-breaching ruptures (e.g., Hill et al., 2012; Sallarès et al., 2021), but our 2-D models (Figures 6–8) and Japan Trench experiment (Figure 10) make it clear that being shallow is not a sufficient reason for the rupture to be anomalously tsunamigenic.

By inference, our results imply that the disproportionately large tsunamis in these events are due to their fault slip being disproportionately large. Satake (1994), Sallarès and Ranero (2019), and many others have shown that failing to account for the very low rigidity of near-trench materials in the common practice of inferring fault slip from seismic records may greatly underestimate the magnitude of shallow slip. If the underestimated slip is enlarged by a factor of two or more to account for the low rigidity, it may be more compatible with the observed tsunami runup (e.g., Geist & Bilek, 2001; Prada et al., 2021; Satake, 1994). However, the cause for the very large slip is not fully understood because fault zone properties also play a vital role (see Section 2.1.2). Besides, a self-consistent mechanism must also account for the long-term slip budget of the megathrust and the availability of elastic strain energy prior to the earthquake. There are also other attempts to explain the geology of tsunami earthquakes by resorting to unusual geometry and rupture style (e.g., Hananto et al., 2020; Hill et al., 2012; Pelayo & Wiens, 1992). Explaining tsunami earthquakes is beyond the scope of this paper, but we think our results have clarified some important concepts and raised important questions for future studies of these events.

6. Conclusions

In this study, we investigate the mechanics of seafloor deformation in megathrust earthquakes and how it influences tsunami runup. To address the question whether buried rupture is intrinsically less tsunamigenic than shallow and trench-breaching rupture, we use a finite element model to simulate elastic crustal deformation and a shallow-water equation model to simulate the ensuing tsunami propagation and runup. Our main findings are summarized as follows.

1. In a megathrust earthquake, tsunamigenic deformation of the upper plate consists of two components: rigid-body translation and elastic thickening. Fundamental to tsunami generation is the trade-off between the two, that is, the enhancement of one component is at the cost of the other. Deformation due to large slip at the trench is dominated by rigid-body translation, such that the horizontal motion of the sloping seafloor greatly enhances seafloor uplift near the trench, but it does not necessarily enhance tsunami runup, because seafloor uplift further landward due to elastic thickening is greatly reduced at the same time (Figures 5–8).
2. The importance of elastic thickening is commonly under-appreciated. For buried ruptures, the updip tapering of fault slip causes elastic shortening and hence bulging of the seafloor with size and shape dependent on the slip gradient and rupture depth (Figure 4). Given slip distribution, there is an "optimal rupture depth" that maximizes elastic thickening and hence the tsunamigenic potential of a buried rupture.
3. Given depth range of a buried rupture, its downdip slip distribution and the resultant variations in slip gradient greatly affect tsunami runup (Figure 8). For ruptures at a relatively shallow depth, greater seaward skewing of the slip distribution, that is, greater concentration of slip near the trench, results in a narrow seafloor bulge near the trench with a gentler land-facing slope which is less potent in causing tsunami runup. The accompanying enhancement of the seaward motion of the sloping seafloor is inadequate to offset this effect.
4. Our synthetic models covering a wide range of geometrical and slip parameters demonstrate that a rupture buried to an optimal depth produces larger seafloor uplift and tsunami runup than almost all the shallower and trench-breaching ruptures with the same peak slip (Ref2 in Figures 5–8). Exceptions occur only when very special rupture geometry is involved, such as a steep frontal thrust cutting through extremely thick trench sediment (Figure 9). Such exceptions are purely hypothetical, because no such special geometry in real subduction zones is expected to persist over a very long distance along strike as implied by 2-D models.

5. Geometrical factors generally do not strongly influence the relative tsunamigenic potential of buried versus trench-breaching ruptures with the same peak slip, although a very steep near-trench seafloor makes the latter a little more tsunamigenic by strengthening the rigid-body translation component (Figure 6). Greater fault dip strengthens elastic thickening and the vertical component of rigid-body translation to enhance seafloor uplift in both rupture types similarly.
6. The theoretical knowledge learned in this study helps us better understand the generation of very large tsunamis such as during the 2011 $M = 9$ Tohoku-oki earthquake. We infer that very large tsunamis require very large slip of the megathrust, not necessarily very shallow and even trench-breaching slip. By hypothetically applying a Tohoku-oki slip model to greater depths, we demonstrated that, if the same large slip were to occur 20 km deeper without breaching the trench, it would generate tsunami runups along the coast facing the area of maximum fault slip no less than observed in 2011. The reason for the very large slip in the 2011 event is an important research subject but is not addressed in this paper.

Data Availability Statement

Tsunami runup data displayed in Figure 10 and Figure S4 of Supporting Information S1 are from The 2011 Tohoku Earthquake Tsunami Joint Survey (TTJS) Group (2011) downloadable from http://www.coastal.jp/tsunami2011. The source data of Figures 6–10 are available at the public research data repository figshare (https://doi.org/10.6084/m9.figshare.20427777.v1).

Acknowledgments
We thank Jiangheng He (Pacific Geoscience Centre) for developing PGCviscl-3D that was used in deformation modeling in this work, Yoshiki Yamazaki (University of Hawai'i at Mānoa) for customizing a NEOWAVE modeling package for us, and Alejandra Gubler (Centro de Investigación para la Gestión Integrada del Riesgo de Desastres, CIGIDEN) for helping us to implement the Kajiura transfer Function script, available at https://github.com/GeoscienceAustralia/ptha, into our model setting. We acknowledge fruitful discussions on theoretical concepts of tsunamis with Kwok Fai Cheung (University of Hawai'i at Mānoa), Patricio Winckler (Universidad de Valparaíso), and Ignacio Sepúlveda (San Diego State University). We thank Dr. Eric Dunham, an anonymous reviewer, and the Associate Editor for their comments. The research was partially supported by the Canada-Chile Leadership Exchange Program of Global Affairs Canada, Iniciativa Científica Milenio (ICM) through Grant NC160025 "Millennium Nucleus CYCLO: The Seismic Cycle Along Subduction Zones", Chile's Fondo Nacional de Desarrollo Científico y Tecnológico, FONDECYT Project 1190258, and Natural Engineering and Science Research Council of Canada Discovery Grant RGPIN-2016-03738 to K. Wang. This is Geological Survey of Canada contribution 20220215.

References

Allen, T., & Hayes, G. (2017). Alternative rupture-scaling relationships for subduction interface and other offshore environments. *Bulletin of the Seismological Society of America*, *107*(3), 1240–1253. https://doi.org/10.1785/0120160255

Carvajal, M., Cisternas, M., & Catalán, P. A. (2017). Source of the 1730 Chilean earthquake from historical records: Implications for the future tsunami hazard on the coast of Metropolitan Chile. *Journal of Geophysical Research: Solid Earth*, *122*(5), 3648–3660. https://doi.org/10.1002/2017jb014063

Carvajal, M., Cisternas, M., Gubler, A., Catalán, P. A., Winckler, P., & Wesson, R. L. (2017). Reexamination of the magnitudes for the 1906 and 1922 Chilean earthquakes using Japanese tsunami amplitudes: Implications for source depth constraints. *Journal of Geophysical Research: Solid Earth*, *122*(1), 4–17. https://doi.org/10.1002/2016jb013269

Carvajal, M., & Gubler, A. (2016). The effects on tsunami hazard assessment in Chile of assuming earthquake scenarios with spatially uniform slip. *Pure and Applied Geophysics*, *173*(12), 3693–3702. https://doi.org/10.1007/s00024-016-1332-x

Cheung, K. F., Lay, T., Sun, L., & Yamazaki, Y. (2022). Tsunami size variability with rupture depth. *Nature Geoscience*, *15*(1), 33–36. https://doi.org/10.1038/s41561-021-00869-z

Du, Y., Ma, S., Kubota, T., & Saito, T. (2021). Impulsive tsunami and large runup along the Sanriku coast of Japan produced by an inelastic wedge deformation model. *Journal of Geophysical Research: Solid Earth*, *126*(8), e2021JB022098. https://doi.org/10.1029/2021jb022098

Felix, R. P., Hubbard, J. A., Moore, J. D., & Switzer, A. D. (2021). The role of frontal thrusts in tsunami earthquake generation. *Bulletin of the Seismological Society of America*, *XX*(2), 1–15. https://doi.org/10.1785/0120210154

Freund, L. B., & Barnett, D. M. (1976). A two-dimensional analysis of surface deformation due to dip-slip faulting. *Bulletin of the Seismological Society of America*, *66*(3), 667–675.

Gao, D., Wang, K., Insua, T. L., Sypus, M., Riedel, M., & Sun, T. (2018). Defining megathrust tsunami source scenarios for northernmost Cascadia. *Natural Hazards*, *94*(1), 445–469. https://doi.org/10.1007/s11069-018-3397-6

GEBCO Bathymetric Compilation Group. (2019). *The GEBCO_2019 Grid-a continuous terrain model of the global oceans and land*. British Oceanographic Data Centre, National Oceanography Centre.

Geist, E. L. (1998). Local tsunamis and earthquake source parameters. *Advances in Geophysics*, *39*, 117–209. https://doi.org/10.1016/s0065-2687(08)60276-9

Geist, E. L. (2002). Complex earthquake rupture and local tsunamis. *Journal of Geophysical Research*, *107*(B5), 2086. https://doi.org/10.1029/2000jb000139

Geist, E. L., & Bilek, S. L. (2001). Effect of depth-dependent shear modulus on tsunami generation along subduction zones. *Geophysical Research Letters*, *28*(7), 1315–1318. https://doi.org/10.1029/2000gl012385

Geist, E. L., Bilek, S. L., Arcas, D., & Titov, V. V. (2006). Differences in tsunami generation between the December 26, 2004 and March 28, 2005 Sumatra earthquakes. *Earth Planets and Space*, *58*(2), 185–193. https://doi.org/10.1186/bf03353377

Geist, E. L., & Dmowska, R. (1999). Local tsunamis and distributed slip at the source. In *Seismogenic and tsunamigenic processes in shallow subduction zones* (pp. 485–512). Birkhäuser.

Gulick, S. P., Austin, J. A., McNeill, L. C., Bangs, N. L., Martin, K. M., Henstock, T. J., et al. (2011). Updip rupture of the 2004 Sumatra earthquake extended by thick indurated sediments. *Nature Geoscience*, *4*(7), 453–456. https://doi.org/10.1038/ngeo1176

Hananto, N. D., Leclerc, F., Li, L., Etchebes, M., Carton, H., Tapponnier, P., et al. (2020). Tsunami earthquakes: Vertical pop-up expulsion at the forefront of subduction megathrust. *Earth and Planetary Science Letters*, *538*, 116197. https://doi.org/10.1016/j.epsl.2020.116197

Hill, E. M., Borrero, J. C., Huang, Z., Qiu, Q., Banerjee, P., Natawidjaja, D. H., et al. (2012). The 2010 Mw 7.8 Mentawai earthquake: Very shallow source of a rare tsunami earthquake determined from tsunami field survey and near-field GPS data. *Journal of Geophysical Research*, *117*(B6), B06402. https://doi.org/10.1029/2012jb009159

Hooper, A., Pietrzak, J., Simons, W., Cui, H., Riva, R., Naeije, M., et al. (2013). Importance of horizontal seafloor motion on tsunami height for the 2011 Mw = 9.0 Tohoku-oki earthquake. *Earth and Planetary Science Letters*, *361*, 469–479. https://doi.org/10.1016/j.epsl.2012.11.013

Hu, Y., & Wang, K. (2008). Coseismic strengthening of the shallow portion of the subduction fault and its effects on wedge taper. *Journal of Geophysical Research*, *113*(B12), B12411. https://doi.org/10.1029/2008jb005724

Hu, Y., & Wang, K. (2012). Spherical-Earth finite element model of short-term postseismic deformation following the 2004 Sumatra earthquake. *Journal of Geophysical Research*, *117*(B5), B05404. https://doi.org/10.1029/2012jb009153

Ikari, M. J., Marone, C., & Saffer, D. M. (2011). On the relationship between fault strength and frictional stability. *Geology*, *39*(1), 83–86. https://doi.org/10.1130/g31416.1

Kajiura, K. (1963). The leading wave of a tsunami. *Bulletin of the Earthquake Research Institute, University of Tokyo*, *41*(3), 535–571.

Kanamori, H. (1972). Mechanism of tsunami earthquakes. *Physics of the Earth and Planetary Interiors*, *6*(5), 346–359. https://doi.org/10.1016/0031-9201(72)90058-1

Kodaira, S., Iinuma, T., & Imai, K. (2021). Investigating a tsunamigenic megathrust earthquake in the Japan Trench. *Science*, *371*(6534). https://doi.org/10.1126/science.abe1169

Kotani, M., Imamura, F., & Shuto, N. (1998). New method of tsunami runup and estimation of damage using GIS data. *Proceedings of the coastal engineering*, (Vol. 45, pp. 356–360). Japan Society of Civil Engineers.

Kozdon, J. E., & Dunham, E. M. (2013). Rupture to the trench: Dynamic rupture simulations of the 11 March 2011 Tohoku earthquake. *Bulletin of the Seismological Society of America*, *103*(2B), 1275–1289. https://doi.org/10.1785/0120120136

Luo, H., & Wang, K. (2021). Postseismic geodetic signature of cold forearc mantle in subduction zones. *Nature Geoscience*, *14*(2), 104–109. https://doi.org/10.1038/s41561-020-00679-9

Ma, S., & Nie, S. (2019). Dynamic wedge failure and along-arc variations of tsunamigenesis in the Japan trench margin. *Geophysical Research Letters*, *46*(15), 8782–8790. https://doi.org/10.1029/2019gl083148

Mori, N., Takahashi, T., Yasuda, T., & Yanagisawa, H. (2011). Survey of 2011 Tohoku earthquake tsunami inundation and run-up. *Geophysical Research Letters*, *38*(7), L00G14. https://doi.org/10.1029/2011gl049210

Mulia, I. E., Heidarzadeh, M., & Satake, K. (2022). Effects of depth of fault slip and continental shelf geometry on the generation of anomalously long-period tsunami by the July 2020 Mw 7.8 Shumagin (Alaska) earthquake. *Geophysical Research Letters*, *49*(3), e2021GL094937. https://doi.org/10.1029/2021gl094937

Pelayo, A. M., & Wiens, D. A. (1992). Tsunami earthquakes: Slow thrust-faulting events in the accretionary wedge. *Journal of Geophysical Research*, *97*(B11), 15321–15337. https://doi.org/10.1029/92jb01305

Polet, J., & Kanamori, H. (2000). Shallow subduction zone earthquakes and their tsunamigenic potential. *Geophysical Journal International*, *142*(3), 684–702. https://doi.org/10.1046/j.1365-246x.2000.00205.x

Prada, M., Galvez, P., Ampuero, J. P., Sallarès, V., Sánchez-Linares, C., Macías, J., & Peter, D. (2021). The influence of depth-varying elastic properties of the upper plate on megathrust earthquake rupture dynamics and tsunamigenesis. *Journal of Geophysical Research: Solid Earth*, *126*(11), e2021JB022328. https://doi.org/10.1029/2021jb022328

Ramos, M. D., & Huang, Y. (2019). How the transition region along the Cascadia megathrust influences coseismic behavior: Insights from 2-D dynamic rupture simulations. *Geophysical Research Letters*, *46*(4), 1973–1983. https://doi.org/10.1029/2018gl080812

Rudnicki, J. W., & Wu, M. (1995). Mechanics of dip-slip faulting in an elastic half-space. *Journal of Geophysical Research*, *100*(B11), 22173–22186. https://doi.org/10.1029/95jb02246

Sallarès, V., Prada, M., Riquelme, S., Meléndez, A., Calahorrano, A., Grevemeyer, I., & Ranero, C. R. (2021). Large slip, long duration, and moderate shaking of the Nicaragua 1992 tsunami earthquake caused by low near-trench rock rigidity. *Science Advances*, *7*(32), eabg8659. https://doi.org/10.1126/sciadv.abg8659

Sallarès, V., & Ranero, C. R. (2019). Upper-plate rigidity determines depth-varying rupture behaviour of megathrust earthquakes. *Nature*, *576*(7785), 96–101. https://doi.org/10.1038/s41586-019-1784-0

Satake, K. (1994). Mechanism of the 1992 Nicaragua tsunami earthquake. *Geophysical Research Letters*, *21*(23), 2519–2522. https://doi.org/10.1029/94gl02338

Satake, K., Fujii, Y., Harada, T., & Namegaya, Y. (2013). Time and space distribution of coseismic slip of the 2011 Tohoku earthquake as inferred from tsunami waveform data. *Bulletin of the Seismological Society of America*, *103*(2B), 1473–1492. https://doi.org/10.1785/0120120122

Scholz, C. H. (1998). Earthquakes and friction laws. *Nature*, *391*(6662), 37–42. https://doi.org/10.1038/34097

Sun, T., Wang, K., Fujiwara, T., Kodaira, S., & He, J. (2017). Large fault slip peaking at trench in the 2011 Tohoku-oki earthquake. *Nature Communications*, *8*(1), 1–8. https://doi.org/10.1038/ncomms14044

Sun, T., Wang, K., & He, J. (2018). Crustal deformation following great subduction earthquakes controlled by earthquake size and mantle rheology. *Journal of Geophysical Research: Solid Earth*, *123*(6), 5323–5345. https://doi.org/10.1029/2017jb015242

Sun, T., Wang, K., Iinuma, T., Hino, R., He, J., Fujimoto, H., et al. (2014). Prevalence of viscoelastic relaxation after the 2011 Tohoku-oki earthquake. *Nature*, *514*(7520), 84–87. https://doi.org/10.1038/nature13778

Tadepalli, S., & Synolakis, C. E. (1994). The run-up of N-waves on sloping beaches. *Proceedings of the Royal Society of London, Series A: Mathematical and Physical Sciences*, *445*, 99–112.

Tanioka, Y., & Satake, K. (1996). Tsunami generation by horizontal displacement of ocean bottom. *Geophysical Research Letters*, *23*(8), 861–864. https://doi.org/10.1029/96gl00736

Tanioka, Y., & Seno, T. (2001). Sediment effect on tsunami generation of the 1896 Sanriku tsunami earthquake. *Geophysical Research Letters*, *28*(17), 3389–3392. https://doi.org/10.1029/2001gl013149

The 2011 Tohoku Earthquake Tsunami Joint Survey Group. (2011). Nationwide field survey of the 2011 off the Pacific coast of tohoku earthquake tsunami. *Journal of Japan Society of Civil Engineers, Series B*, *67*(1), 63–66. https://doi.org/10.2208/kaigan.67.63

Tsuji, T., Kawamura, K., Kanamatsu, T., Kasaya, T., Fujikura, K., Ito, Y., et al. (2013). Extension of continental crust by anelastic deformation during the 2011 Tohoku-oki earthquake: The role of extensional faulting in the generation of a great tsunami. *Earth and Planetary Science Letters*, *364*, 44–58. https://doi.org/10.1016/j.epsl.2012.12.038

Wang, K., & He, J. (2008). Effects of frictional behavior and geometry of subduction fault on coseismic seafloor deformation. *Bulletin of the Seismological Society of America*, *98*(2), 571–579. https://doi.org/10.1785/0120070097

Wang, K., & Hu, Y. (2006). Accretionary prism in subduction earthquake cycles: The theory of dynamic Coulomb wedge. *Journal of Geophysical Research*, *111*(B6), B06410. https://doi.org/10.1029/2005JB004094

Wang, K., Hu, Y., & He, J. (2012). Deformation cycles of subduction earthquakes in a viscoelastic Earth. *Nature*, *484*(7394), 327–332. https://doi.org/10.1038/nature11032

Wang, K., Sun, T., Brown, L., Hino, R., Tomita, F., Kido, M., et al. (2018). Learning from crustal deformation associated with the M9 2011 Tohoku-oki earthquake. *Geosphere*, *14*(2), 552–571. https://doi.org/10.1130/ges01531.1

Wang, K., & Tréhu, A. M. (2016). Invited review paper: Some outstanding issues in the study of great megathrust earthquakes—The Cascadia example. *Journal of Geodynamics*, *98*, 1–18. https://doi.org/10.1016/j.jog.2016.03.010

Wang, P. L., Engelhart, S. E., Wang, K., Hawkes, A. D., Horton, B. P., Nelson, A. R., & Witter, R. C. (2013). Heterogeneous rupture in the great Cascadia earthquake of 1700 inferred from coastal subsidence estimates. *Journal of Geophysical Research: Solid Earth*, *118*(5), 2460–2473. https://doi.org/10.1002/jgrb.50101

Wang, X., & Power, W. L. (2011). COMCOT: A tsunami generation propagation and run-up model. *GNS Science*.

Ward, S. N. (1980). Relationships of tsunami generation and an earthquake source. *Journal of Physics of the Earth*, *28*(5), 441–474. https://doi.org/10.4294/jpe1952.28.441

Williamson, A., Melgar, D., & Rim, D. (2019). The effect of earthquake kinematics on tsunami propagation. *Journal of Geophysical Research: Solid Earth*, *124*(11), 11639–11650. https://doi.org/10.1029/2019jb017522

Witter, R. C., Zhang, Y. J., Wang, K., Priest, G. R., Goldfinger, C., Stimely, L., et al. (2013). Simulated tsunami inundation for a range of Cascadia megathrust earthquake scenarios at Bandon, Oregon, USA. *Geosphere*, *9*(6), 1783–1803. https://doi.org/10.1130/ges00899.1

Yamazaki, Y., Cheung, K. F., & Kowalik, Z. (2011). Depth-integrated, non-hydrostatic model with grid nesting for tsunami generation, propagation, and run-up. *International Journal for Numerical Methods in Fluids*, *67*(12), 2081–2107. https://doi.org/10.1002/fld.2485

Yamazaki, Y., Cheung, K. F., & Lay, T. (2018). A self-consistent fault slip model for the 2011 Tohoku earthquake and tsunami. *Journal of Geophysical Research: Solid Earth*, *123*(2), 1435–1458. https://doi.org/10.1002/2017jb014749